



Estimation of radiative effect of a heavy dust storm over northwest China using Fu–Liou model and ground measurements



Wencai Wang^a, Jianping Huang^{a,*}, Tian Zhou^a, Jianrong Bi^a, Lei Lin^a,
Yonghang Chen^{a,b}, Zhongwei Huang^a, Jing Su^a

^a Key Laboratory for Semi-Arid Climate Change of the Ministry of Education, College of Atmospheric Sciences, Lanzhou University, Lanzhou 730000, PR China

^b College of Environmental Science and Engineering, Donghua University of China, Shanghai 201620, PR China

ARTICLE INFO

Article history:

Received 2 August 2012

Received in revised form

16 October 2012

Accepted 22 October 2012

Available online 3 November 2012

Keywords:

Dust aerosol

Radiative forcing

Fu–Liou model

ABSTRACT

A heavy dust storm that occurred in Northwestern China during April 24–30 2010 was studied using observational data along with the Fu–Liou radiative transfer model. The dust storm was originated from Mongolia and affected more than 10 provinces of China. Our results showed that dust aerosols have a significant impact on the radiative energy budget. At Minqin (102.959°E, 38.607°N) and Semi-Arid Climate and Environment Observatory of Lanzhou University (SACOL, 104.13°E, 35.95°N) sites, the net radiative forcing (RF) ranged from 5.93 to 35.7 W m⁻² at the top of the atmosphere (TOA), -6.3 to -30.94 W m⁻² at surface, and 16.77 to 56.32 W m⁻² in the atmosphere. The maximum net radiative heating rate reached 5.89 K at 1.5 km on 24 April at the Minqin station and 4.46 K at 2.2 km on 29 April at the SACOL station. Our results also indicated that the radiative effect of dust aerosols is affected by aerosol optical depth (AOD), single-scattering albedo (SSA) and surface albedo. Modifications of the radiative energy budget by dust aerosols may have important implications for atmospheric circulation and regional climate.

Crown Copyright © 2012 Published by Elsevier Ltd. All rights reserved.

1. Introduction

Dust aerosol has a strong radiative forcing (RF) of the climate system, modulating convective processes and the formation and lifetime of clouds and thereby influencing the global and regional climate change. Asian dust is generally generated in Outer and Inner Mongolia, Taklimakan Desert and the Gobi Desert, most frequently in late winter and early spring, and then transported eastward.

The RF due to Mineral dust has been studied by researchers over the world. RF by anthropogenic aerosols is predicted to induce strong regional cooling over east and South Asia [1], Australian, Mediterranean [2], German and Indian [3]. Huang et al. [4] found that the average

daily mean net RF of a dust storm over Taklimakan desert was 44.4, -41.9, and 86.3 W m⁻², at the top of the atmosphere (TOA), at the surface, and in the atmosphere, respectively. Le et al. [5] found that the direct shortwave (SW) radiation effect of Saharan dusts at solar zenith angle 21.68° was 53.48 ± 8.56 W m⁻² per unit aerosol optical depth. Ge et al. [6] estimated that the dust aerosol RF over northwestern China ranges from -7.9 to -35.8 W m⁻², comparable to results reported from East Asia and Africa. Helmert et al. [7] found that a mean shortwave radiative efficiency of -196 W m⁻² for prevalently reflecting dust particles and -220 W m⁻² for prevalently absorbing dust particles at the surface in the southern Sahara. They determined a shortwave dust forcing efficiency at the TOA of -121 W m⁻² close to the source areas and -55 W m⁻² at larger distance. Mallet et al. [8] found a positive effect of dust aerosols on net longwave radiation on TOA over the entire West

* Corresponding author.

E-mail address: hjp@lzu.edu.cn (J. Huang).

Africa; they determined an increase between 20 and 50 W m^{-2} . Santese et al. [9] found that the daily-mean SW forcing is offset by the LW forcing of $\sim 30\%$ at the surface and of $\sim 50\%$ at the TOA. Li et al. [10] showed that nationwide annual and diurnal mean RF is found to be $-15.7 \pm 8.9 \text{ W m}^{-2}$ at the surface, $0.3 \pm 1.6 \text{ W m}^{-2}$ at the TOA, and $16.0 \pm 9.2 \text{ W m}^{-2}$ inside the atmosphere in China. Stanelle et al. [11] analyzed the radiative efficiency of dust particles, for shortwave radiation at the surface they found a radiative efficiency of -140 W m^{-2} . At TOA the influence of dust particles depends strongly on surface albedo. At the surface the increase of the net longwave radiative fluxes is about 79 W m^{-2} for a dust layer with an AOD of 1. If such a dust layer is present the increase of net longwave radiative fluxes is approximately 26 W m^{-2} at TOA. From the discussion above we conclude that the largest forcing values are usually located over or near dust sources.

In addition to the effects of dust aerosols described above, dust aerosols also warm the atmosphere and cool the surface through the absorption and reflection of radiation. Huang et al. [4] found that dust aerosols have a significant impact on the radiative energy budget over the Taklimakan desert. Under light, moderate and heavy dust conditions, dust aerosols heat the atmosphere by up to 1, 2 and 3 K day^{-1} , respectively (daily mean values); the maximum daily mean radiative heating rate reaches 5.5 K day^{-1} at 5 km. Other studies [12,13] indicated that during the daytime, dust aerosols can warm the atmosphere between 0.3 and 4 K day^{-1} , on average, depending on altitude and latitude. Strong warming (i.e., heating rates as high as 8 K day^{-1}) was also observed locally within a limited portion of the dust plume.

The magnitude of dust direct radiative effect (DRE) depends on the distribution of dust aerosol optical properties and the scattering and absorbing properties of the environment, specifically, on the aerosol extinction coefficient, the single-scattering albedo (SSA), the asymmetry parameter and the phase function [14]. While aerosol optical depth and size are relatively well constrained, uncertainties in the aerosol SSA [15] and vertical profile [16,17] contribute significantly to overall uncertainties in DRE, especially for all-sky estimates. On a global basis, direct aerosol radiative forcing at the TOA is generally determined to be negative. On a regional scale, the magnitude and sign of dust aerosol RF are significantly different depending on the SSA. Dust aerosols have a negative TOA forcing for large SSA, and a positive TOA forcing for small SSA [14,18–20].

Larger uncertainties exist in current estimates of aerosol forcing because of incomplete knowledge concerning the distribution and the physical and chemical properties of aerosols as well as aerosol–cloud interactions [21]. Many of the studies of dust terrestrial RF use idealized aerosol properties at these wavelengths. One reason for this has been the almost total lack of observations of optical properties of dust in the terrestrial data [12]. The refractive indices used in many climate models are those of the “dust-like” aerosol of the World Climate Program (WCP) [22] and are based on Volz [23]. The uncertainty for the aerosol direct climate forcing is about

a factor of 2–3 whereas that for the indirect forcing is much larger and difficult to quantify [24]. These uncertainties raise questions about the interpretation of the 20th century temperature record [25] and complicate the assessment of aerosol impacts on surface–atmosphere interactions, the atmospheric boundary layer [26], global surface air temperatures [27–30], the hydrological cycle [31], photochemistry [32], and ecosystems [33].

Thus, there is clearly a need for better measuring the dust aerosol's physical and optical properties within the solar and the terrestrial spectrum [34]. Fortunately, a field experiment was conducted over Minqin in Gansu Province (102.959°E , 38.607°N) to examine the dust aerosol's optical properties and radiative effects during April to June, 2010. Minqin is becoming one of China's largest source areas for dust due to its severely degraded environment. Based on the observational data of field experiment, we can get the accurate input parameters for Fu–Liou radiative model, such as the SSA, asymmetry factor, surface albedo and extinction coefficients of dust aerosol by Micro-pulse Lidar system (MPL).

In this paper, the Fu–Liou radiative transfer model [35,36] was used to compute the aerosol radiative heating rates and RF using the surface observation data as input parameters, which extends our previous study [4,37–41]. The ground-based measurements, used in conjunction with the Fu–Liou radiative model, should lead to a reliable analysis of dust aerosol effects on the radiative energy budget and thus improve our understanding of the impact of dust aerosols on climate.

2. Data and model

An intensive field experiment was conducted over Minqin in Gansu Province (102.959°E , 38.607°N) to investigate the dust aerosol's optical properties and radiative effects during April to June, 2010. The SACOL's Mobile Facility (SMF) was deployed with a set of state-of-the-art instruments, including Precision Spectral Pyranometer (PSP), Normal Incidence Pyrheliometer (NIP, Eppley Lab. and CHP1, Kipp and Zonen), CIMEL sun photometer (CE-318) and the Multi-Filter Rotating Shadowband Radiometer (MFRSR). The unshaded and shaded PSP were used to measure the total and diffuse irradiances, respectively. The direct normal irradiance was measured by both the NIP and CHP1 mounted on a Kipp and Zonen two axis sun tracker (2AP). This field campaign provides us an opportunity to study the dust aerosols effect in Northwestern China.

2.1. Lidar and radiation data

2.1.1. Lidar data

Aerosol vertical distribution (normalized relative backscatter and depolarization ratio) is measured using the Micro-pulse Lidar system (MPL). MPL is a safe, compact, and maintenance-free lidar system originally developed by Spinhirne [42] for acquiring long-term data sets of backscatter profiles of aerosols and clouds [43]. MPL uses an Nd: YLF pulsed laser diode that operates at a wavelength of 527 nm. The continual aerosol and cloud measurements were acquired with a 30-m-range resolution

and a 1-min time average. In our study, we used the MPL to observe the vertical distribution of aerosols. Additionally, the National Institute for Environmental Studies (NIES) Mie lidar observation data from SACOL was used to study the vertical profiles of dust.

2.1.2. The Clouds and the Earth's Radiant Energy System (CERES) and surface radiation monitoring system

The CERES Single Scanner Footprint (SSF) instantaneous measurements include radiance, radiative flux at the surface and the TOA, and a variety of parameters describing the clear and cloudy portions of the footprint [44]. The CERES scanning broadband radiometers measure broadband SW (0.2–5.0 μm) and total radiances, which are used to determine the TOA SW and LW (5–100 μm) fluxes using anisotropic correction models [45]. These depend on the surface and cloud properties within the radiometer field of view. The scene types within each CERES scanner footprint were determined by analyzing collocated, high-resolution imager data. The instantaneous uncertainties in the CERES SW and LW TOA fluxes were 5–10% and less than 3%, respectively [46].

The surface-radiation monitoring system consisted of upward and downward pyranometers (CM21, Kipp and Zonen) for incoming and outgoing shortwave radiation, and upward and downward pyrgeometers (CG4, Kipp and Zonen) for incoming and outgoing longwave radiation. All radiation quantities were sampled each second but taken at a 1-min time resolution. The datasets were quality checked via the Baseline Surface Radiation Network quality-control procedure [47]. Furthermore, a set of redundant broadband pyranometers were deployed side by side for quality-control purposes. The disagreements among different instruments remained within 10 W m^{-2} .

To estimate the accuracy of the Fu–Liou model using the input parameters from observations, we compared the SW and LW flux from the surface radiation monitoring system and CERES with the results simulated by the Fu–Liou model at the surface and TOA.

2.2. Surface observations

The column-integrated spectral aerosol measurements at Minqin in this study were made with the sky radiometer (Model POM-02, manufactured by PREDE Co., Ltd.). The PREDE sky radiometer is one of the key instruments which is widely used in the SKYNET—aerosol–cloud–radiation interaction ground-based observation network in East Asia [48]. The sky radiometer measures the solar direct irradiance and the radiance from the sky within a 1.0° full field of view in eleven bands at 315, 340, 380, 400, 500, 675, 870, 940, 1020, 1600, 2200 nm every 10 min [49]. The surface albedo in the context is related to the broadband surface albedo. The mean broadband surface albedo for SW (0.305–4.2 μm) at Minqin and SACOL are obtained from surface-radiation monitoring system, which is calculated by the ratio of upward SW radiation and downward SW. The downward shortwave incoming (hereafter, denotes as DSW) and the upward

reflected SW radiation (hereafter, denotes as USW) are measured with a uplooking and a downlooking pyranometer (CM21; 0.3–3.0 μm), respectively.

The aerosol properties at SACOL were measured by the Cimel Electronique CE-318 sun photometer that is the Aerosol Robotic Network (AERONET) standard instrument. CE-318 is an automatic direct solar and sky radiometer with spectral interference filters (10 nm FWHM) centered on the wavelengths selected for aerosol measurements (440, 670, 870, and 1020 nm) [50]. The sun photometer works by measuring the intensity of the solar radiation reaching the surface in the specified wavelength bands and then converting it to optical depth using the corresponding intensities at the TOA. The maximum AERONET uncertainty in aerosol optical depth (AOD) retrieval was estimated to be 0.02 [51]. Single scattering albedos (SSAs) are expected to have an uncertainty of 0.03–0.05 and the uncertainty of asymmetry parameter is about 0.04 depending on aerosol type and loading [52]. In this paper, we use the Level1.5 quality-assured data sets of AERONET (<http://aeronet.gsfc.nasa.gov>). Bi et al. [53] compared the AOD at 500 nm derived from Cimel sun photometer and PREDE sky radiometer at Minqin and concluded that the difference of AOD measured by Cimel and PREDE can be achieved with ± 0.02 during the measurement in 2010. Che et al. [54] indicated that single-scattering albedos estimated from sky radiometer are 0.03, 0.06, and 0.07 larger than those provided by AERONET at 670, 870, and 1020 nm.

We used SKYNET (Level 2.2) and AERONET to provide model parameters such as AOD, SSA, and asymmetry factor at Minqin and SACOL. The mean broadband surface albedos were obtained from the aforementioned surface-radiation monitoring system, which were 0.29 and 0.18 for Minqin and SACOL during the whole measurement, respectively. The mean SSA and asymmetry factor at Minqin were 0.91 and 0.71 at 675 nm, respectively, and those at SACOL were 0.91 and 0.70 at 675 nm. We could see that the mean SSA at Minqin and SACOL were the same, and our historical data showed that the difference between the sky radiometer and AERONET was about 6% for SSA at 675 nm.

2.3. Fu–Liou radiative transfer model

We used the Fu–Liou radiative transfer model to estimate the RF and heating rate in a cloud-free atmosphere with and without a dust aerosol layer. The radiative transfer model was originally developed by Fu and Liou [35,36] and modified by Rose and Charlock [55]. There is also unavoidable error for Fu–Liou model. Generally speaking, the delta-four-stream is accurate than delta-two-stream, so here we used delta-four-stream approximation. The model has fifteen spectral bands from 0.175 to 4.0 μm in the SW and twelve LW spectral bands between 2850 and 0 cm^{-1} . The surface albedo, AOD, SSA and other aerosol parameters were taken from SKYNET at Minqin and AERONET at SACOL. For a given time and location, the pressure, temperature, and water vapor profiles were interpolated from the reanalysis product of the National Centers for Environmental Prediction and

National Center for Atmospheric Research (NCEP/NCAR). The ozone concentration was acquired from the NCEP Stratospheric Monitoring Group Ozone Blended Analysis (SMOBA) product based on solar backscatter ultraviolet (SBUV) and TIROS Operational Vertical Sounder (TOVS) observations. We selected the transported aerosol type [4] in this study.

3. Dust case

A strong dust storm event occurred in the north-western China during 24–27 April 2010. Fig. 1 shows the strong dust storm by Total Sky Imager (TSI-880) on 24 April 2010 at Minqin in Gansu Province. The TSI-880 is a full-color camera with a software package that offers

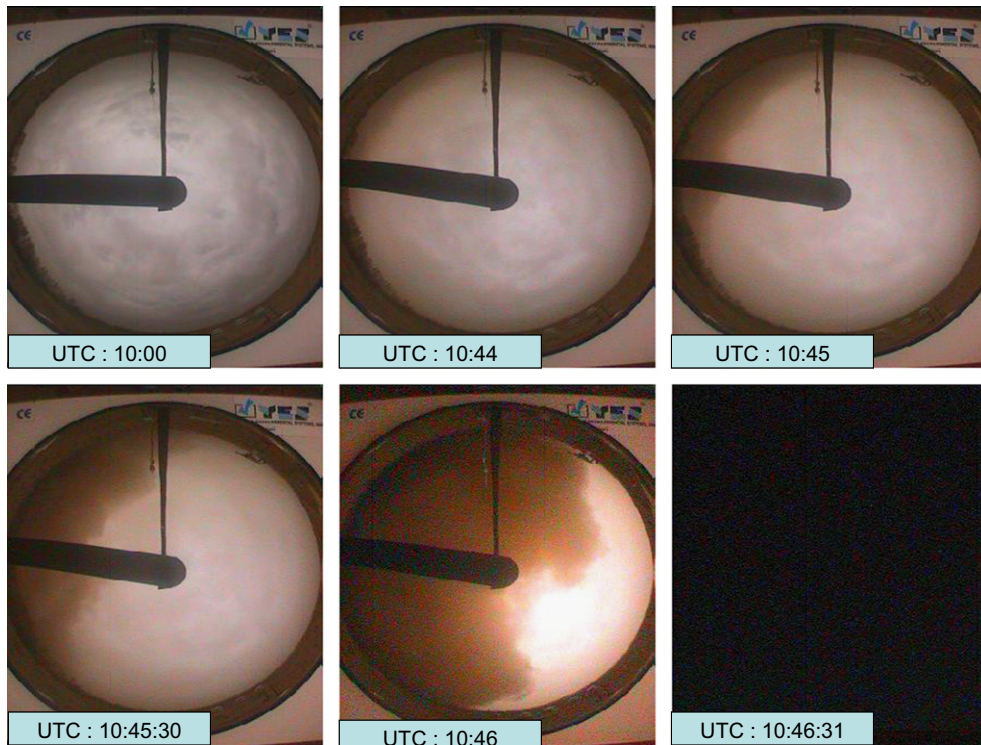


Fig. 1. The strong dust storm case observed by a total sky imager on Minqin station on April 24, 2010.

Table 1

Dust storm intensity, horizontal visibility, wind direction, wind speed, and occurrence time at Hexi Corridor, Gansu Province, from surface meteorological records.

Station	Latitude	Longitude	Dust storm intensity	Horizontal visibility (m)	Wind direction	Wind speed (m/s)	Occurrence time (local time)
Dunhuang	40.09	94.41	Dust storm	600	Northwest	17	09:15
Yumen	40.16	97.02	Dust storm	900	Northwest	20	12:47
Jinta	40.00	98.54	Dust storm	900	Northwest	27	14:26
Subei	39.49	94.89	Dust storm	600	Northwest	12.6	17:02
Jiuquan	39.46	98.29	Super strong dust storm	0	Northwest	26	20:37
Dingxin	40.18	99.31	Super strong dust storm	40	Northwest	22	15:34
Linze	39.14	100.17	Strong dust storm	50	Northwest	20	16:06
Sunan	38.86	99.57	Dust storm	600	Northwest	16.7	16:23
Zhangye	38.56	100.26	Super strong dust storm	40	Northwest	22	16:27
Gaotai	39.22	99.50	Strong dust storm	500	Northwest	22	17:00
Shandan	38.48	101.05	Strong dust storm	200	West	22	17:06
Minle	38.43	100.85	Strong dust storm	50	Northwest	24	17:18
Minqin	38.38	103.05	Super strong dust storm	0	Northwest	28	19:35
Jinchang	38.28	102.10	Strong dust storm	200	West Northwest	20.8	21:55

an easy-to-use and reliable field sensor for sky imaging. Fig. 1 shows that it was cloudy at UTC 10:00 on 24 April 2010. At UTC 10:44, dust aerosols appeared from the

northwest direction. The aerosols moved eastward, masking three quarters of the sky at UTC 10:46. By UTC 10:46:31, the entire sky was masked by dust aerosols, and horizontal

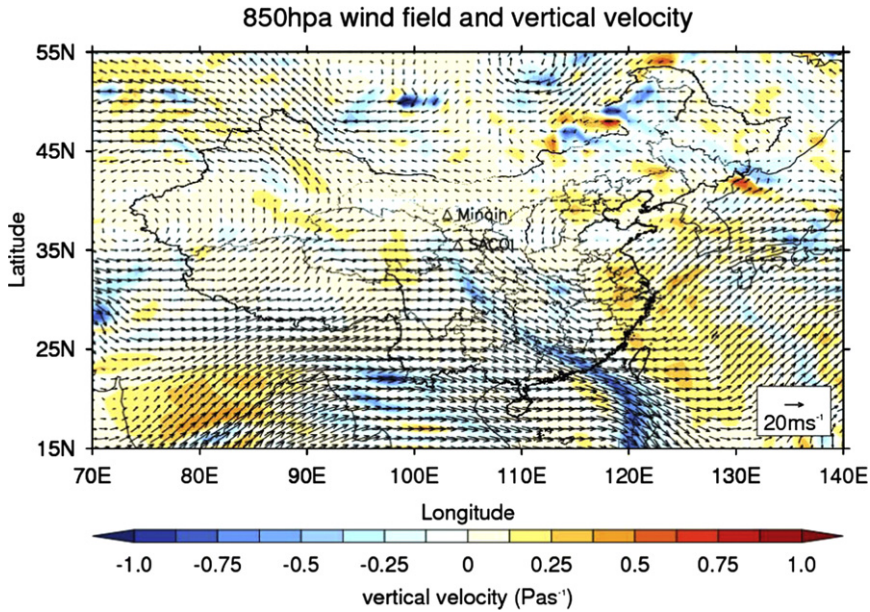


Fig. 2. The wind field (black arrows) and vertical velocity (color scales) at 850 hPa level at UTC 06 on April 24, 2010. (For interpretation of the references to color in this figure legend, the reader is referred to the web version of this article.)

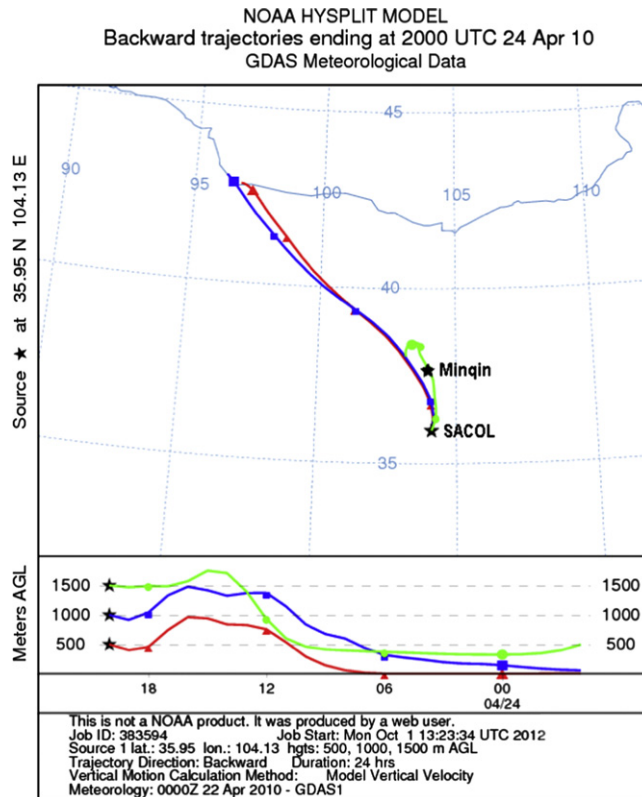


Fig. 3. Horizontal (top) and vertical (bottom) components of the backward trajectories of the dust storm at 2000 UTC, April 24, 2010, originated at the SACOL (lower asterisk) station, for three altitudes of 500 m (red color), 1000 m (blue color), and 1500 m (green color) (produced with HYSPLIT). (For interpretation of the references to color in this figure legend, the reader is referred to the web version of this article.)

visibility was nearly 0 m. The maximum instant wind speed reached 28 m/s during the dust storm. From the TSI observation, it only took 2 min and 31 s for dust aerosols to mask the entire sky. As this dust event was intense, we called it the black storm. The black storm lasted for 2 h, and the dust storm lasted until 27 April at Minqin, resulting in great disruption to traffic and daily life there.

Table 1 shows the surface meteorological records for 24 April 2010 in Hexi Corridor, Gansu Province. Generally speaking, the dust storm with a wind speed level greater and equal to nine and the visibility range from 50 m to 200 m, we call it strong dust storm. The dust storm with instant wind speed greater and equal to 25 m/s and the visibility less and equal 50 m, we call it super dust storm.

From Table 1 we can see that five stations observed dust storms and strong dust storms, while four stations observed a super-strong dust storm. During the dust storm, the horizontal visibility was less than 40 m, and the maximum instantaneous wind speed reached 28 m/s. Moreover, the horizontal visibility at Minqin and Jiuquan was nearly 0 m. In the following days, the dust storm was

transported to Eastern China and affected Shanxi, Hebei, and more than 10 other provinces and cities.

Fig. 2 shows the 850-hPa wind field and vertical velocity. A strong convergence occurred in Mongolia, suggesting that the dust storm may originate there. Additionally, the wind direction was mainly from the west and northwest, causing the transport of dust aerosols from west to east.

A backward trajectory analysis of the same time period was conducted to find the source region and transport path of the dust aerosols (as shown in Fig. 3). The NOAA/Air Resources Laboratory HYSPLIT model was used to calculate the 24-h backward trajectories of the air masses at SACOL at 20:00 UTC on 24 April. The Global Data Assimilation System (GDAS) meteorological dataset of the NCEP was used as input. Two arrival points (at the SACOL and Minqin stations) were selected in the altitude range of 500–1500 m (500, 1000, and 1500 m) above ground level (AGL). The green and blue lines represent the 1000–1500-m back trajectories, which indicate that the dust originated over Mongolia on 24 April 2010 (or somewhat earlier). It was then transported

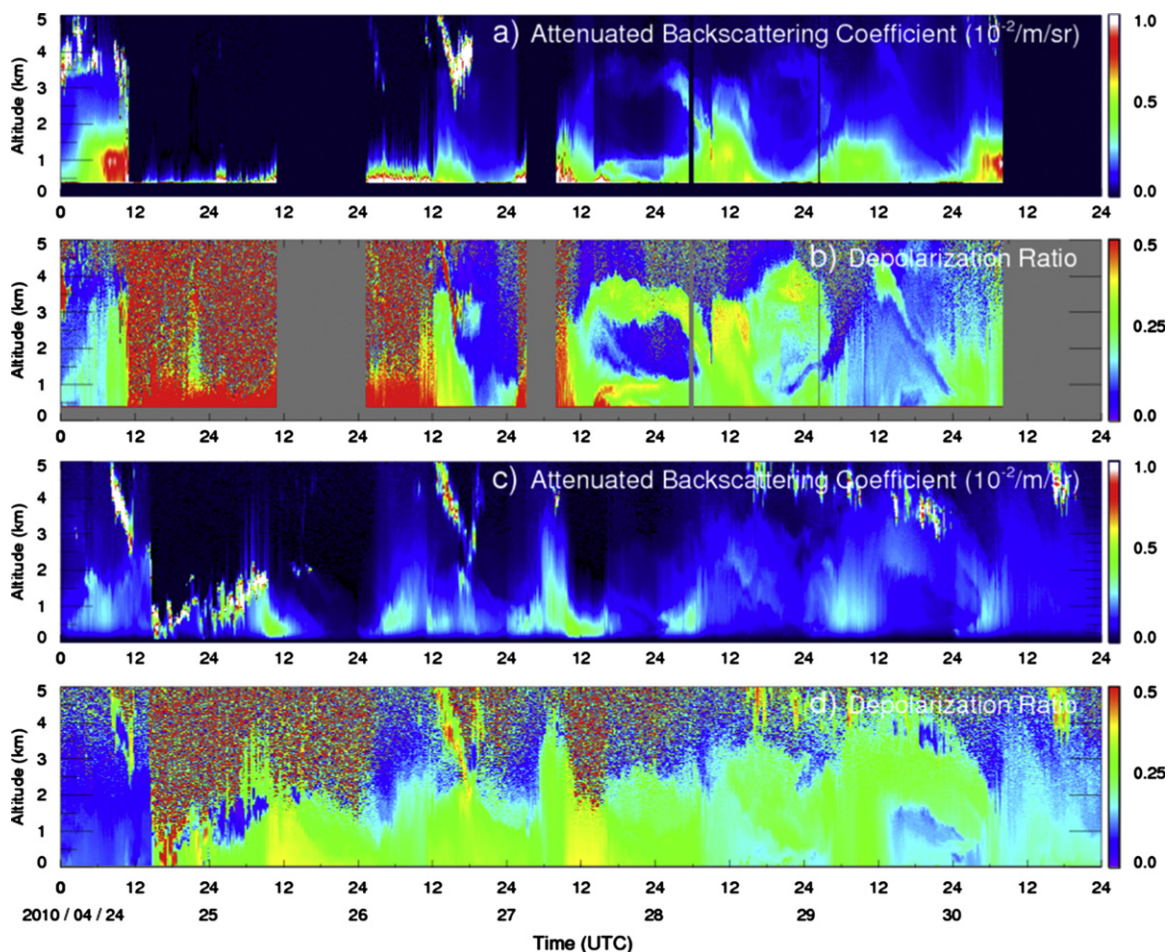


Fig. 4. The MPL normalized relative backscatter and depolarization ratio at Minqin (a and b) and NIES Lidar normalized relative backscatter and depolarization ratio (c and d) at SACOL for the dust event during April 24–30, 2010.

from Minqin and other regions to SACOL. Because the dust storm occurred in Minqin at 10:46 UTC on 24 April, the HYSPLIT information indicates that the dust aerosols took 8–9 h to travel to SACOL.

Fig. 4 shows typical dust observations taken during 24–30 April 2010 by the MPL at Minqin and NIES lidar at SACOL (the gap in Fig. 4 is no signal regions where MPL and NIES Lidar had no signal due to the strong dust storm). The depolarization ratio of dust is high due to the non-spherical shape of the particles, whereas for other types of aerosols, the depolarization ratio is low (close to zero). The depolarization ratio is used as an indicator to separate dust from other aerosol types [56]. From the vertical information in Fig. 4a–d, we can see that there were sharp increases in attenuated backscattering coefficients and depolarization ratios at both Minqin and SACOL on 24 April. At Minqin (Fig. 4a and b), the dust storm happened at about 10:46 UTC and was severe. Similar observations at SACOL, shown in Fig. 4c and d, indicate that the dust event occurred at SACOL at about 14:40 UTC. Moreover, the dust storm at Minqin lasted until 27 April and was stronger than that at SACOL. However, the altitude of the dust layer at SACOL was higher than that in Minqin, indicating that when the dust aerosols were transported from Minqin and other regions to SACOL, the strength decreased, but the altitude increased.

4. Dust aerosol radiative heating and forcing effects

As discussed before, the aerosol input parameters for the Fu–Liou model were obtained from surface observation and the pressure, temperature, and water vapor vertical profiles from NCEP, the extinction coefficient vertical profile derived from Lidar Equation using Fernald Method [57]. We compared the modeled simultaneous results with CERES and surface observations (shown in Fig. 5). Fig. 5a and c compares the modeled simultaneous surface downward SW/LW fluxes with radiometer observations. Fig. 5b and d compares the modeled simultaneous TOA upwards SW/LW with CERES observations during 24–30 April at Minqin and SACOL. The simulated surface downward SW/LW fluxes agreed reasonably closely with those from radiometer observations. The averaged differences between model and surface observations were only 4.43 and 1.1 W m^{-2} for SW and LW, respectively. At the TOA, the averaged differences between the model and CERES observations were also small (only 1.11 and 0.2 W m^{-2} for SW and LW respectively). Therefore, it is clear from this comparison that the radiative-transfer model can be used to reliably determine the RF and vertical heating rate with input from surface observations.

Fig. 6 gives the temporal average evolution of the mean AOD, SSA and asymmetry from April 22 to 30,

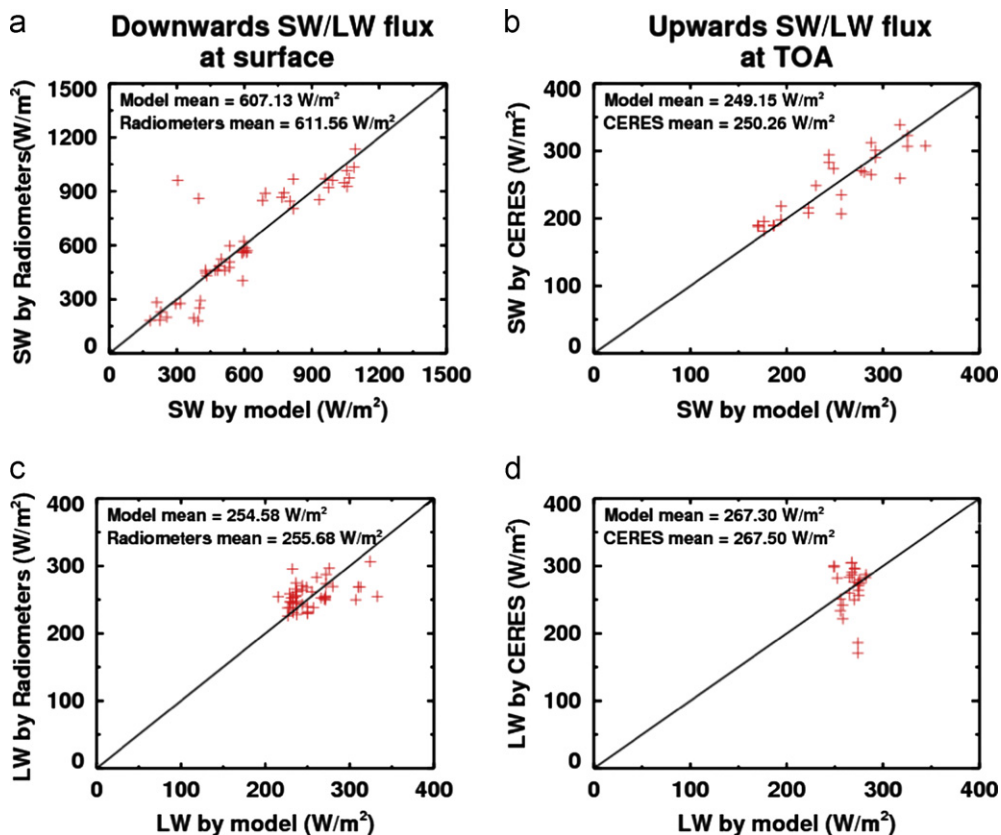


Fig. 5. The modeled simultaneous downward surface SW (a) and LW (c) fluxes versus surface observations, and the modeled simultaneous TOA upwards SW (b) and LW (d) fluxes versus satellite CERES observations during April 24–30 on Minqin and SACOL.

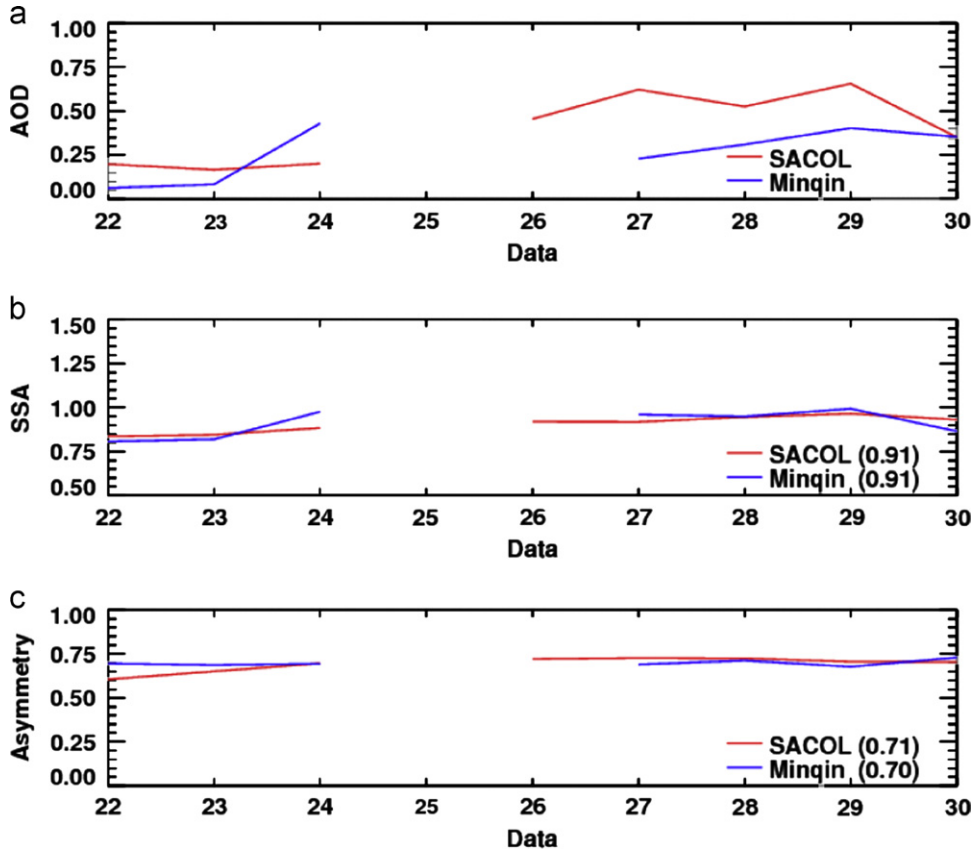


Fig. 6. Daily averaged of the AOD (a), SSA (b) and asymmetry (c) from April 22 to 30, 2010 along with the SSA and ASY mean values at SACOL and Minqin.

2010 at Minqin and SACOL. The aerosol optical depths in Fig. 6 are observed by the SKYNET and AERONET. Fig. 4 shows that there were some missing data due to the strong dust storm at Minqin. So here we just compared the mean values of aerosol optical depth when Minqin and SACOL both had data in Fig. 6, although the dust storm at Minqin may be stronger than at SACOL, the optical depth at Minqin may be less than SACOL due to the missing data. Fig. 6a shows that the mean AOD sharply increased on April 24 at both Minqin and SACOL. Moreover, the mean AOD at SACOL was larger than that at Minqin after April 24, but the SSA at SACOL was smaller than that in Minqin after April 24 (Fig. 6b). This implied that when the dust aerosols were transported from Minqin and other regions to SACOL, they may have mixed with anthropogenic pollutants such as sulfate and nitrate; these interactions cause the aerosols to be more soluble and increased their chance to serve as cloud condensation nuclei [58]. Fig. 7 gives the averaged dust aerosol RF at the TOA, at the surface, and in the atmosphere for the cases in this study at the Minqin and SACOL stations.

The LW and SW flux are defined both for the TOA and the surface as

$$T_{lw} = F_{lw}^{down} - F_{lw}^{up}$$

$$T_{sw} = F_{sw}^{down} - F_{sw}^{up}$$

the aerosol RF is given as

$$A_{lw} = T_{lw}^a - T_{lw}^{clr}$$

$$A_{sw} = T_{sw}^a - T_{sw}^{clr}$$

$$A_{net} = A_{lw} + A_{sw}$$

where F_{lw}^{down} (F_{lw}^{up}) and F_{sw}^{down} (F_{sw}^{up}) are the downwind (upward) LW and SW fluxes, respectively. The indices 'a' and 'clr' denote the existence of dust aerosols and clear-sky scenes without dust aerosols.

Fig. 7a–c shows the RF values at the Minqin station. At the TOA, dust aerosols had a warming effect in the LW, SW, and net flux. The maximum net warming was 35.70 W m^{-2} on April 24. At the surface, dust aerosols had a positive LW RF but negative values for the SW and net RF. Dust aerosols cooled the surface by decreasing the incident SW radiation but warmed it through dust-emitted LW radiation. The net result at the surface was a cooling effect, and the maximum cooling was -17.78 W m^{-2} on April 24. In the atmosphere, the dust aerosols had a cooling effect for LW but a warming effect for SW. The net effect was warming, and the maximum net RF was 53.48 W m^{-2} on April 24. Fig. 7d–f shows the same conclusion. The results in Fig. 7 indicates that both SW and LW radiation forcing of dust aerosols played important roles in the radiative energy budget at the TOA, at the surface, and in the atmosphere.

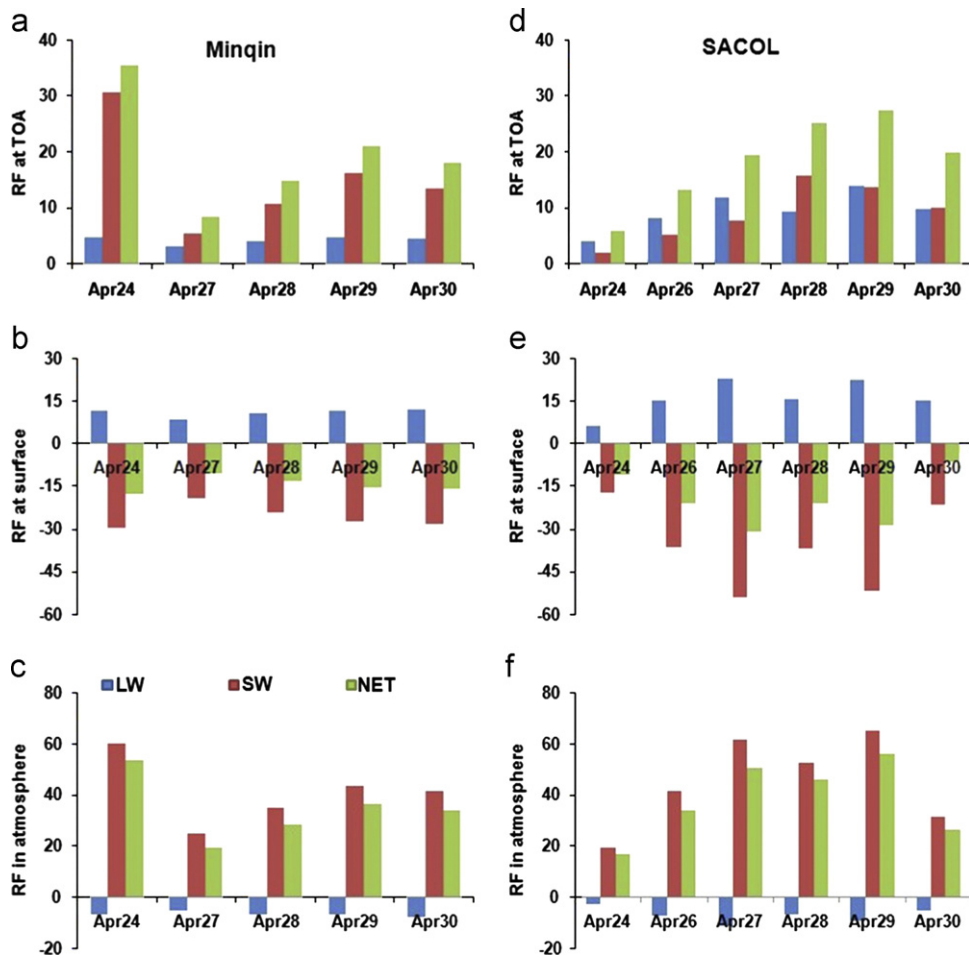


Fig. 7. Daily mean radiative forcing (RF) of dust aerosols at the TOA, at the surface, and in the atmosphere at Minqin and SACOL. Units: $W m^{-2}$.

The mean RFs at the TOA, surface, and atmosphere as a function of the AOD at Minqin and SACOL are given in Fig. 8. The mean absolute values of the TOA, surface, and atmosphere RF increased with increasing AOD. Additionally, the absolute values of RF at SACOL were larger than those at Minqin in the same AOD bin. This implies that when dust aerosols were transported from Minqin and other regions to SACOL, they mixed with the cross-area pollution aerosol, increasing the AOD but decreasing the SSA, resulting in greater radiation effects of dust aerosols at SACOL than at Minqin.

Fig. 9 shows the impact of dust aerosols daily averaged LW, SW, and net heating rates. These values were obtained as the differences between the simulated radiative heating rates with and without dust aerosols. The dust aerosols appear to have had little effect on the LW radiative heating rates at Minqin and SACOL. They show a warming effect above the surface, but they cooled in the dust layers and above the dust layer. The maximum warming, which occurred near the surface, was typically about 0.51 K at Minqin and 0.57 K at SACOL. The maximum cooling was typically about -1.07 K at Minqin and -0.87 K at SACOL. Dust aerosols appear to show a warming effect in and above the dust layer. The maximum net aerosol

heating rate was 5.89 K at 1.5 km on 24 April at Minqin and 4.64 K at 2.2 km on 29 April at SACOL. Because there was a super dust storm in Minqin on 24 April, the heating and cooling rates there were larger than the values in SACOL.

5. Uncertainties in RF

Although we attempted to minimize errors by using the observations as model input, the estimated dust RF may still have had some unavoidable uncertainties. Estimation of the uncertainties in RF at different levels in the atmosphere (TOA, in the atmosphere and at the surface) is therefore important for understanding the context of the results.

Table 2 summarizes the results of a sensitivity analysis for the case studies presented in this paper. Based on the instrument uncertainty, the errors in the AOD were estimated to be on the order of 10%. The surface albedo also varied by 10%, the asymmetry varied by 5%, and the SSA varied by 6%. Since the dust storm mainly occurred near the surface (see Fig. 4), and the dust aerosols touched the surface, so here we just discussed the perturbing of increasing height, and we increased the height of dust

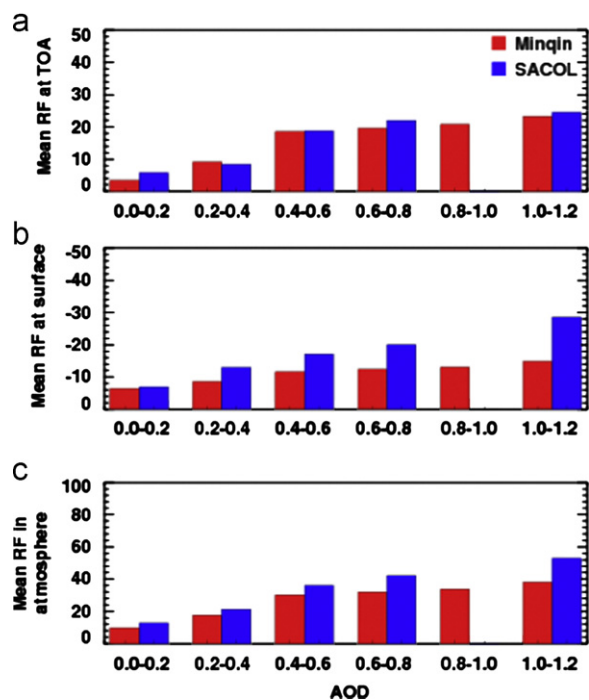


Fig. 8. Daily mean aerosol radiative forcing at the top of the atmosphere (a), surface (b) and in the atmosphere (c) as a function of AOD at Minqin (red) and SACOL (blue). (For interpretation of the references to color in this figure legend, the reader is referred to the web version of this article.)

aerosol by 0.5 km. We believe that the above uncertainties represent the maximum range of possible values.

The results in Table 2 show that the SW RF estimates were sensitive to the surface albedo, AOD, and SSA, while the LW estimates were somewhat less sensitive to changes in SSA and AOD at the TOA, at the surface, and in the atmosphere. The changes in the surface albedo reduced the magnitude of the net RF by about 1.7% and –1.8% in the atmosphere. The variations in the AOD resulted in changes of –1.3% and 1.9%, variations in the asymmetry resulted in changes of $\pm 3.72\%$, and the variations in SSA resulted in changes of $\pm 4.1\%$. At the TOA, the variations in surface albedo, AOD, asymmetry, and SSA resulted in changes of 4.9% and –3.55%, –9.8% and 11.4%, $\pm 8.92\%$, and $\pm 12.5\%$ in the net RF, respectively. Furthermore, the variations in the four parameters resulted in changes in the surface net RF of 3.2% and –1.75%, –8.5% and 9.5%, $\pm 5.2\%$, $\pm 8.4\%$. The variations in aerosol height resulted in changes of 0.26%, –0.62% and 0.88% at the TOA, surface and in the atmosphere, respectively. The changes in the SSA had a larger impact on the aerosol RF at the TOA, whereas moderate errors in the estimates of the AOD, asymmetry, the surface albedo and aerosol height. In addition, the larger dust particles may fall to surface when transported from Minqin to SACOL. As we know that the difference in dust particles size can cause the differences in optical thickness retrieval and RF computation, thus the difference in dust particles between Minqin and SACOL is also one of the factors that affect the RF.

6. Discussion and conclusions

Dust aerosols are an important part of the Earth's climate system. They influence the radiative energy budget through direct, indirect, and semi-direct effects. They also affect cloud microphysical properties. Aerosol environmental and climatic effects have become an important scientific issue.

Our study showed that the maximum mean net RF at Minqin was 35.70, –17.78, and 53.48 W m^{-2} , respectively, at the TOA, at the surface, and in the atmosphere on April 24, 2010. At SACOL the corresponding values were 27.52, –28.80, and 56.32 W m^{-2} at the TOA, at the surface, and in the atmosphere, respectively, on April 29, 2010. Dust aerosols can absorb and scatter solar SW and absorb and emit LW radiation and hence affect RF in complex ways. The effect of dust aerosols depends on many factors, such as surface albedo, and AOD, SSA. Our results indicate that the most important factors for LW forcing in the atmosphere are the AOD and its vertical distribution which was derived from Lidar Equation using Fernald Method, whereas SW is dependent on the surface albedo, AOD, and SSA. Generally speaking, dust aerosols have a positive (larger surface albedo) or negative (smaller surface albedo) effect on SW at the TOA but a negative effect at the surface because the existence of dust aerosols reduces the incident SW radiation. For LW radiation, dust aerosols have a positive effect both at the TOA and at the surface. In the atmosphere, dust aerosols have a negative effect on LW but a positive effect on SW. The net effect is positive, heating the atmosphere. In dusty atmospheric layers, the dust typically heats the layer by up to 3–6 K, depending on the dust concentration. The maximum net (SW+LW) radiative rate reached 5.89 K at 1.5 km on April 24 at Minqin and 4.46 K at 2.2 km on April 29 at SACOL.

Dust aerosols had a larger mean AOD at SACOL than that at Minqin on April 24, when the super dust storm occurred there. However, the mean SSA at SACOL was smaller than that at Minqin during April 22–29, when the dust storm occurred. This implies that when dust aerosols were transported from Minqin and other regions to SACOL, their optical properties may have changed. Additionally, dust aerosols at SACOL had larger absolute RF values than did those at Minqin with the same AOD. Because the mean SSA was 0.91 at both Minqin and SACOL, the uncertainty between the sky radiometer at Minqin and AERONET at SACOL was about 6% based on our history measurement data. The mean difference in RF between Minqin and SACOL at the TOA, at the surface, and in the atmosphere was greater than the uncertainties shown in Table 2. The HYSPLIT simulation also confirmed that dust aerosols were transported from Minqin to SACOL, and also from some other regions to SACOL (not shown here). Thus, when dust aerosols were transported from Minqin and other regions to SACOL, they may have been mixed with polluted aerosols, increasing their effect on radiation. However, the radiation is affected by many factors, such as the surface albedo, and vertical profile.

Dust aerosols can significantly affect the regional climate by heating the air column. This modifies the vertical thermal structure, atmospheric stability, and

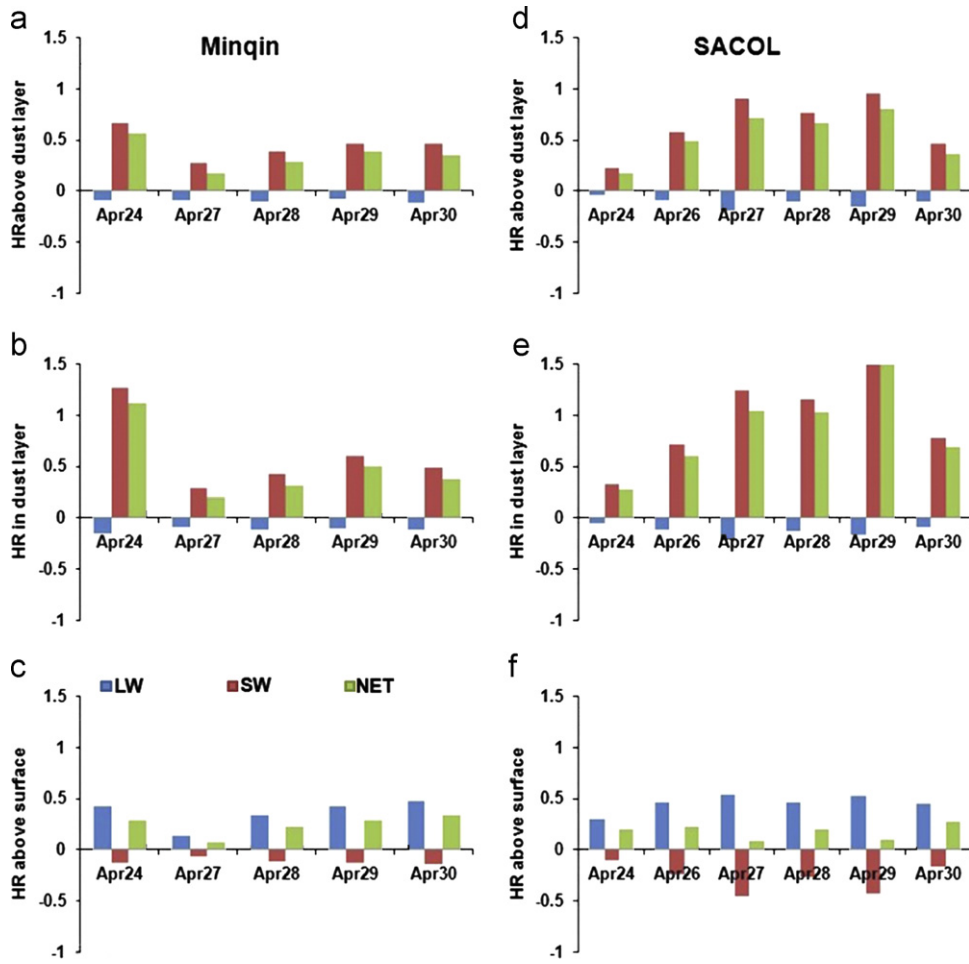


Fig. 9. Daily mean heating rate (HR) above, in the dust layers and above surface at Minqin and SACOL. Units: K.

Table 2

Analysis of the sensitivity of the Fu–Liou radiative transfer model for radiative forcing at the TOA, at the surface, and in the atmosphere. Units: $W m^{-2}$ (case studies discussed in the text).

	Deviation from baseline forcing (%)								
	TOA			Surface			Atmosphere		
	LW	SW	NET	LW	SW	NET	LW	SW	NET
Albedo – 10%	0	4.9	4.9	0	3.2	3.2	0	1.7	1.7
Albedo + 10%	0	–3.55	–3.55	0	–1.75	–1.75	0	–1.8	–1.8
AOD – 10%	–2.3	–7.5	–9.8	–1.2	–7.3	–8.5	–1.1	–0.2	–1.3
AOD + 10%	2.6	8.8	11.4	1.8	7.7	9.5	0.8	1.1	1.9
SSA – 6%	1.2	11.3	12.5	–1.3	9.7	8.4	2.5	1.6	4.1
SSA + 6%	–1.2	–11.3	–12.5	1.3	–9.7	–8.4	–2.5	–1.6	–4.1
ASY – 5%	4.3	4.62	8.92	1.4	3.8	5.2	2.9	0.82	3.72
ASY + 5%	–4.3	–4.62	–8.92	–1.4	–3.8	–5.2	–2.9	–0.82	–3.72
H + 0.5 km	0.21	0.05	0.26	–0.46	–0.16	–0.62	0.67	0.21	0.88

convection strength and affects regional precipitation patterns [59]. Dust aerosols also have a large effect on the surface energy budget, atmospheric circulation, and even global climate change. Dust aerosol radiative effects are

important in modulating global and regional climate. They affect heating rate and thereby convective processes, the formation and lifetime of clouds, and the distribution of chemical constituents, and they are a major environmental

and public health concern in China. Therefore, further research should focus on combining satellite measurements, surface measurements, and model simulations.

Acknowledgments

This work was jointly supported by the National Basic Research Program of China (2012CB955301), the National Science Foundation of China under Grant 41175134, the Program for Changjiang Scholars and Innovative Research Team in University (IRT1018), the Fundamental Research Funds for the Central Universities (Izujbky-2011-145), the National Natural Science Foundation of China (No. 40975012) and supported by Foundation of Key Laboratory for Semi-Arid Climate Change of the Ministry of Education in Lanzhou University. We are grateful to Prof. Nakajima for supplying SKYRAD software. AERONET/CERES data supplied by NASA are greatly appreciated. We gratefully acknowledge the NOAA Air Resources Laboratory (ARL) for the provision of the HYSPLIT transport and dispersion model and/or READY website (<http://www.arl.noaa.gov/ready.html>). We would also like to thank all SACOL team members for the instrument establishing and maintaining.

References

- Chen W, Liao H, Seinfeld JH. Future climate impacts of direct radiative forcing of anthropogenic aerosols, tropospheric ozone, and long-lived greenhouse gases. *J Geophys Res* 2007;12:D14209. <http://dx.doi.org/10.1029/2006JD008051>.
- Bergamo A, Tafuro AM, Kinne S, De Tomasi F, Perrone MR. Monthly-averaged anthropogenic aerosol direct radiative forcing over the Mediterranean based on AERONET aerosol properties. *Atmos Chem Phys* 2008;8:6995–7014.
- Ramanathan V, Li F, Ramana MV, Praveen PS, Kim D, Corrigan CE, et al. Atmospheric brown clouds: hemispherical and regional variations in long-range transport, absorption, and radiative forcing. *J Geophys Res* 2007;112:D22S21. <http://dx.doi.org/10.1029/2006JD008124>.
- Huang JP, Minnis P, Yan HR, Yi YH, Chen B, Zhang L, et al. Taklimakan dust aerosol radiative heating derived from CALIPSO observations using the Fu–Liou radiation model with CERES constraints. *Atmos Chem Phys* 2009;9:4011–21.
- Li R, Min QL, Harrison LC. A case study: the indirect aerosol effects of mineral dust on warm clouds. *J Atmos Sci* 2010;67:805–16.
- Ge JM, Su J, Ackerman TP, Fu Q, Huang JP, Shi JS. Dust aerosol optical properties retrieval and radiative forcing over northwestern China during the 2008 China–U.S. joint field experiment. *J Geophys Res* 2010;115:D00K12. <http://dx.doi.org/10.1029/2009JD013263>.
- Helmert J, Heinold B, Tegen L, Hellmuth O, Wendisch M. On the direct and semi-direct effect of Saharan dust over Europe: a modeling study. *J Geophys Res* 2007;112:D13208. <http://dx.doi.org/10.1029/2006JD007444>.
- Mallet M, Tulet P, Serca D, Solmon F, Dubovik O, Pelon J, et al. Impact of dust aerosols on the radiative budget, surface heat fluxes, heating rate profiles and convective activity over West Africa during March 2006. *Atmos Chem Phys* 2009;9:7143–60. <http://dx.doi.org/10.5194/acp-9-7143-2009>.
- Santese M, Perrone MR, Zakey AS, De Tomasi F, Giorgi F. Modeling of Saharan dust outbreaks over the Mediterranean by RegCM3: case studies. *Atmos Chem Phys* 2010;10:133–56.
- Li Z, Lee K, Wang Y, Xin J, Hao W. First observation-based estimates of cloud-free aerosol radiative forcing across China. *J Geophys Res* 2010;115:D00K18. <http://dx.doi.org/10.1029/2009JD013306>.
- Stanelle T, Vogel B, Vogel H, Bäumer D, Kottmeier C. Feedback between dust particles and atmospheric processes over West Africa during dust episodes in March 2006 and June 2007. *Atmos Chem Phys* 2010;10:10771–88.
- Satheesh SK, Vinoj V, Moorthy KK. Vertical distribution of aerosols over an urban continental site in India inferred using a micro pulse lidar. *Geophys Res Lett* 2006;33:L20816. <http://dx.doi.org/10.1029/2006GL027729>.
- Lemaître C, Flamant C, Cuesta J, Raut J-C, Chazette P, Formenti P, et al. Radiative heating rates profiles associated with a springtime case of Bodélé and Sudan dust transport over West Africa. *Atmos Chem Phys* 2010;10:8131–50. <http://dx.doi.org/10.5194/acp-10-8131-2010>.
- Huang JP, Wang TH, Wang WC, Li ZQ. Dust–cloud–precipitation interactions over Asian arid and semi-arid regions. *Atmos Res*, submitted for publication.
- Loeb NG, Su WY. Direct aerosol radiative forcing uncertainty based on a radiative perturbation analysis. *J Climate* 2010;23:5288–93.
- Zarzycki CM, Bond TC. How much can the vertical distribution of black carbon affect its global direct radiative forcing? *Geophys Res Lett* 2010;37:L20807. <http://dx.doi.org/10.1029/2010GL044555>.
- Huang JF, Zhang CD, Prospero JM. African dust outbreaks: a satellite perspective of temporal and spatial variability over the tropical Atlantic Ocean. *J Geophys Res* 2010;115:D05202. <http://dx.doi.org/10.1029/2009JD012516>.
- Takemura T, Nakajima T, Dubovik O, Holben BN, Kinne S. Single-scattering albedo and radiative forcing of various aerosol species with a global three-dimensional model. *J Climate* 2002;15:333–52.
- Pandithurai G, Dipu S, Dani KK, Tiwari S, Bisht DS, Devara PCS, et al. Aerosol radiative forcing during dust events over New Delhi, India. *J Geophys Res* 2008;113:D13209. <http://dx.doi.org/10.1029/2008JD009804>.
- McFarlane SA, Kassianov EI, Barnard J, Flynn C, Ackerman TP. Surface shortwave aerosol radiative forcing during the atmospheric radiation measurement mobile facility deployment in Niamey, Niger. *J Geophys Res* 2009;114:D00E06. <http://dx.doi.org/10.1029/2008JD010491>.
- Yu H, Kaufman YJ, Chin M, Feingold G, Remer LA, Anderson TL, et al. A review of measurement-based assessments of the aerosol direct radiative effect and forcing. *Atmos Chem Phys* 2006;6:613–66. <http://dx.doi.org/10.5194/acp-6-613-2006>.
- World Climate Program (WCP). A preliminary cloudless standard atmosphere for radiation computation. Geneva: World Meteorology Organization; 1986.
- Volz FE. Infrared optical constants of ammonium sulphate, Sahara dust, volcanic pumice and flyash. *Appl Opt* 1973;12:564–7.
- Haywood J, Boucher O. Estimates of the direct and indirect radiative forcing due to tropospheric aerosols: a review. *Rev Geophys* 2000;38:513–43.
- Anderson TL, Charlson RJ, Schwartz SE, Knutti R, Boucher O, Rodhe H, et al. Climate forcing by aerosols—a hazy picture. *Science* 2003;300:1103–4.
- Yu H, Liu SC, Dickinson RE. Radiative effects of aerosols on the evolution of the atmospheric boundary layer. *J Geophys Res* 2002;107(D12):4142. <http://dx.doi.org/10.1029/2001JD000754>.
- Charlson RJ, Schwartz SE, Hales JH, Cess RD, Coakley Jr. JA, Hansen JE, et al. Climate forcing by anthropogenic aerosols. *Science* 1992;255:423–30.
- Penner JE, Dickinson RE, O'Neill CA. Effects of aerosol from biomass burning on the global radiation budget. *Science* 1992;256:1432–4.
- Kiehl JT, Briegleb BP. The relative role of sulfate aerosols and greenhouse gases in climate forcing. *Science* 1993;260:311–4.
- Hansen J, Sato M, Ruedy R. Radiative forcing and climate response. *J Geophys Res* 1997;102:6831–64.
- Ramanathan V, Crutzen PJ, Kiehl JL, Rosenfeld D. Aerosols, climate, and the hydrological cycle. *Science* 2001;294:2119–24.
- Dickerson RR, Kondragunta S, Stenchikov G, Civerolo KL, Doddridge BG, Holben BN. The impacts of aerosols on solar ultraviolet radiation and photochemical smog. *Science* 1997;278:827–30.
- Chameides WL, Yu H, Liu SC, Bergin M, Zhou X, Mearns L, et al. A case study of the effects of atmospheric aerosols and regional haze on agriculture: an opportunity to enhance crop yields in China through emission controls? *Proc Natl Acad Sci* 1999;96(24):13626–33.
- Sokolik LN, Winker DM, Bergametti G, Gillette DA, Carmichael G, Kaufman YJ, et al. Introduction to special section: outstanding problems in quantifying the radiative impacts of mineral dust. *J Geophys Res* 2001;106:18015–27.
- Fu Q, Liou KN. On the correlated k-distribution method for radiative transfer in nonhomogeneous atmosphere. *J Atmos Sci* 1992;49:2139–56.
- Fu Q, Liou KN. Parameterization of the radiative properties of cirrus clouds. *J Atmos Sci* 1993;50:2008–25.

- [37] Huang JP, Minnis P, Lin B, Wang TH, Yi YH, Hu YX, et al. Possible influences of Asian dust aerosols on cloud properties and radiative forcing observed from MODIS and CERES. *Geophys Res Lett* 2006;33:L06824. <http://dx.doi.org/10.1029/2005GL024724>.
- [38] Huang JP, Lin B, Minnis P, Wang TH, Wang X, Hu YX, et al. Satellite-based assessment of possible dust aerosols semi-direct effect on cloud water path over East Asia. *Geophys Res Lett* 2006;33:L19802. <http://dx.doi.org/10.1029/2006GL026561>.
- [39] Wang WC, Huang JP, Minnis P, Hu YX, Li JM, Huang ZW, et al. Dusty cloud properties and radiative forcing over dust source and downwind regions derived from A-train data during the Pacific dust experiment. *J Geophys Res* 2010;115:D00H35. <http://dx.doi.org/10.1029/2010JD014109>.
- [40] Huang ZW, Huang JP, Bi JR, Wang GY, Wang WC, Fu Q, et al. Dust aerosol vertical structure measurements using three MPL lidars during 2008 China–U.S. joint dust field experiment. *J Geophys Res* 2010;115:D00K15. <http://dx.doi.org/10.1029/2009JD013273>.
- [41] Wang TH, Huang JP. A method for estimating optical properties of dusty cloud. *Chin. Opt. Lett.* 2009;7(5):368–72.
- [42] Spinhirne JD. Micro pulse lidar. *IEEE Trans Geosci Remote Sens* 1993;31:48–55. <http://dx.doi.org/10.1109/36.210443>.
- [43] Welton EJ, Campbell JR, Spinhirne JD, Scott III VS. Global monitoring of clouds and aerosols using a network of micro pulse LIDAR systems. *Proc SPIE Int Soc Opt Eng* 2001;4893:151–8.
- [44] Wielicki BA, Barkstorm BR, Harrison EF, Lee III RB, Smith GL, Cooper JE. Clouds and the Earth's radiant energy system (CERES): an earth observing system experiment. *Bull Am Meteor Soc* 1996;77:853–68.
- [45] Loeb NG, Kato S, Loukachine K, Manalo-Smith N. Angular distribution models for top-of-atmosphere radiative flux estimation from the clouds and Earth's radiant energy system instrument on the Terra satellite. Part 1: methodology. *J Atmos Ocean Technol* 2005;22:338–51.
- [46] Loeb GN, Kato S, Loukachine K, Manalo-Smith N, Doelling DR. Angular distribution models for top-of-atmosphere radiative flux estimation from the clouds and the Earth's radiant energy system instrument on the Terra satellite. Part II: validation. *J Atmos Oceanic Technol* 2007;24:564–84.
- [47] Ohmura A, Dutton EG, Forgan B, Fröhlich C, Gilgen H, Hegner H, et al. Baseline surface radiation network (BSRN/WCRP), a new precision radiometry for climate research. *Bull Am Meteorol Soc* 1998;79:2115–36.
- [48] Takamura T, Takenaka H, Cui Y, Nakajima TY, Higurashi A, Fukuda S, et al. Aerosol and cloud validation system based on SKYNET observations: estimation of shortwave radiation budget using ADEOS-II/GLI data. *J Remote Sens Soc Jpn* 2009;29:40–53.
- [49] Uchiyama A, Yamazaki A, Togawa H, Asano J. Characteristics of aeolian dust observed by sky-radiometer in the intensive observation period 1 (IOP1). *J Meteor Soc Jpn* 2005;83A:291305.
- [50] Carlos T, Cachorro V, Berjon A, Sorribas M, Vergaz R, Defrutos A, et al. Aerosol optical depth at ALOMAR observatory (Andøya, Norway) in summer 2002 and 2003. *Tellus B* 2006;58:218–28.
- [51] Eck TF, Holben BN, Reid JS, Dubovik O, Smirnov A, O'Neill NT, et al. Wavelength dependence of the optical depth of biomass burning, urban, and desert dust aerosol. *J Geophys Res* 1999;104(D24):31333–49.
- [52] Dubovik O, King MD. A flexible inversion algorithm for the retrieval of aerosol optical properties from Sun and sky radiance measurements. *J Geophys Res* 2000;105(D16):20673–96.
- [53] Bi J, Huang J, Fu Q, Ge J, Shi J, Zhou T, et al. Field measurement of clear-sky solar irradiance in Badain Jaran Desert of Northwestern China. *J Quant Spectrosc Radiat Transfer*. <http://dx.doi.org/10.1016/j.jqsrt.2012.07.025>, this issue.
- [54] Che H, Shi G, Uchiyama A, Yamazaki A, Chen H, Goloub P, et al. Intercomparison between aerosol optical properties by a PREDE skyradiometer and CIMEL sunphotometer over Beijing, China. *Atmos Chem Phys* 2008;8:3199–214.
- [55] Rose FG, Charlock TP. New Fu–Liou code tested with ARM Raman lidar and CERES in pre-CALIPSO exercise. In: Extended abstract for 1st conference on atmospheric radiation (AMS). Ogden, Utah, USA; 3–7 June 2002.
- [56] Murayama T, Takenaka H, Cui Y, Nakajima TY, Higurashi A, Fukuda S, et al. Ground-based network observation of Asian dust events of April 1998 in east Asia. *J Geophys Res* 2001;106(D16):18345–60.
- [57] Fernald FG. Analysis of atmospheric lidar observations: some comments. *Appl Opt* 1984;23:652–3. <http://dx.doi.org/10.1364/AO.23.000652>.
- [58] Levin Z, Ganor E, Gladstein V. The effects of desert particles coated with sulfate on rain formation in the eastern Mediterranean. *J Appl Meteorol* 1996;35:1511–23.
- [59] Gu Y, Liou KN, Chen W, Liao H. Direct climate effect of black carbon in China and its impact on dust storms. *J Geophys Res* 2010;115:D00K14. <http://dx.doi.org/10.1029/2009JD013427>.